

Supermassive black hole binaries in gaseous and stellar circumnuclear discs: orbital dynamics and gas accretion.

M. Dotti¹, M. Colpi², F. Haardt¹, & L. Mayer^{3,4}

¹ Dipartimento di Fisica e Matematica, Università dell'Insubria, Via Valleggio 11, 22100 Como, Italy

² Dipartimento di Fisica G. Occhialini, Università degli Studi di Milano Bicocca, Piazza della Scienza 3, 20126 Milano, Italy

³ Institute for Theoretical Physics, University of Zurich, CH-8057, Zurich, Switzerland

⁴ Institute of Astronomy, Department of Physics, ETH, Zurich, Wolfgang-Pauli Strasse, HC-8095 Zurich, Switzerland

arXiv:astro-ph/0612505v1 18 Dec 2006

26 May 2019

ABSTRACT

The dynamics of two massive black holes in a rotationally supported nuclear disc of mass $M_{\text{disc}} = 10^8 M_{\odot}$ is explored using N-Body/SPH simulations. Gas and star particles are co-present in the disc. Described with a Mestel profile, the disc has a vertical support provided by turbulence of the gas, and by stellar velocity dispersion. A primary black hole of mass $4 \times 10^6 M_{\odot}$ is placed at the centre of the disc, while a secondary black hole is set initially on an eccentric co-rotating orbit in the disc plane. Its mass is in a 1 to 1, 1 to 4, and to 10 ratio, relative to the primary. With this choice, we mimic the dynamics of black hole pairs released in the nuclear region at the end of a gas-rich galaxy merger. It is found that, under the action of dynamical friction, the two black holes form a close binary in ~ 10 Myrs. The inspiral process is insensitive to the mass fraction in stars and gas present in the disc and is accompanied by the circularization of the orbit. We have revealed the occurrence of radial inflows around each individual black hole that can create small gaseous Keplerian disc weighing $\sim 2\%$ of the black hole mass, and of size ~ 0.01 pc. The mass of the tightly (loosely) bound particles increases (decreases) with time as the black holes spiral into closer and closer orbits. Double AGN activity is expected to occur on an estimated timescale of $\lesssim 10$ Myrs, comparable to the inspiral timescale. The double nuclear point-like sources that may appear during dynamical evolution have typical separations of $\lesssim 10$ pc.

Key words: black hole physics – hydrodynamics – galaxies: starburst – galaxies: evolution – galaxies: nuclei

1 INTRODUCTION

Collisions of gas-rich spirals may lead to the formation of (ultra-) luminous infrared galaxies (U-LIRGs) that are observed in different phases of their evolution. NGC 6240 is the example of a system in its “early” stage of merging, as it is composed of two star-burst spiral galaxies that overlap. NGC 6240 shows also the presence of two spatially resolved X-ray sources, separated in projection by ~ 1.4 kpc. Their SED indicates that the emission comes from two active, massive black holes (MBHs) powered by accretion (Komossa et al. 2003; Risaliti et al. 2006). One additional system that indicates the presence of an active MBH pair is Arp 299, observed in its early (Ballo et al. 2004) in this early state.

The majority of (U-)LIRGs however appears in the “later” phase of the merger, when the remnant is settling into dynamical equilibrium. (U-)LIRGs are still accompanied by an intense burst of star formation that sustains the

high infrared luminosity observed (see for a review Sanders & Mirabel 1996). What is remarkable in these systems is the presence of a rotationally supported, central massive gaseous disc (up to $10^{10} M_{\odot}$) that extends on scales of ~ 100 pc (Sanders & Mirabel 1996; Scoville et al. 1997; Downes & Solomon 1998; Tacconi et al. 1999; Bryant & Scoville 1999; Greve et al. 2006). During the encounter, gas-dynamical and gravitational torques drive large amounts of gas in the core of the remnant where the MBHs are expected to reside (Barnes & Hernquist 1991, 1996; Kazantzidis et al. 2005).

The formation and evolution of MBH binaries in merging galaxies have a large number of potentially interesting astrophysical consequences, e.g., the creation of galactic cores (Milosavljevic et al. 2002), the ejection of hyper-velocity stars (Yu & Tremaine 2003; Brown et al. 2006) and the production of gravitational waves detectable by *LISA* (Hughes 2002; Bender et al. 2004; Sesana et al. 2005). MBH binaries can also produce peculiar AGN features like peri-

odic modulations, double activity (as mentioned above), and wiggling jets (see Komossa 2006 for a review).

Cosmologically motivated simulations of gas-rich galaxy mergers with MBHs (Kazantzidis et al. 2005; Mayer et al. 2006) have shown that large scale inflows ensue in the individual galaxies, after first pericentre passage, leading to the formation of nuclear discs around the MBHs (as observed in ‘‘early type’’ mergers). Only later, when the merger comes to completion, a circum–nuclear massive disc forms with characteristics consistent with that seen in ‘‘late type’’ (U–)LIRGs (Mayer et al. 2006). In the disc, the MBHs pair closely, forming a mildly eccentric Keplerian binary. It is this late phase that we wish to explore further in this paper.

In our previous work (Dotti, Colpi & Haardt 2006, hereafter DCH06), we studied the dynamical evolution of MBH pairs embedded in a circum–nuclear gaseous disc (see also Escala et al. 2005) studying different MBH mass ratios and initial orbital eccentricities. It was shown that the during MBH inspiral the orbit circularizes under the action of gas–dynamical friction, and that around each MBH a large overdensity, driven by the MBH’s gravity, was tightly coupled to their motion.

In the simulations presented in DCH06, the gaseous disc was embedded into a larger scale spherically symmetric stellar distribution. Fragmentation of the disc was prevented by using an adiabatic equation of state and star formation was, simply, neglected. However, our simulations did not consider the possible co–presence of an axisymmetric nuclear stellar population. Indeed, nuclear stellar discs are observed in many early and late type galaxies (van den Bosch et al. 1998; Scorsa & van den Bosch 1998; Morelli et al. 2004; Krajnovic & Jaffe 2004; Lopes et al. 2006). A stellar disc is likely the end–product of a nuclear gaseous star–forming disc, resulting from galaxy mergers and/or, from the secular evolution of bars (Krajnovic & Jaffe 2004; Kormendy et al. 2005; Ferrarese et al. 2006). Two observations of young stellar discs in NGC1068 and NGC 1097 are presented in Davies et al. (2006). They estimate stellar masses of $10^8 M_\odot$, disc radii of ~ 50 pc, and a vertical scale height of $5 - 10$ pc, suggesting that the star’s velocity dispersion provides significant pressure support.

In this paper, in order to study the role of a nuclear stellar disc in driving the orbital evolution of the MBH binary, we run a new series of simulations of MBH pairs embedded in a disc, allowing the gas to be (partially) converted into stars. Our stellar discs mimic the ones observed by Davies et al. (2006). The ultimate aim is to detail the dynamics of the MBHs inside the stellar and gaseous disc and the gas–dynamics in the surroundings of the each individual MBH.

An important improvement of our new runs with respect to DCH06 and other similar simulations (Kazantzidis et al. 2005) lies in the sizable increase in the numerical resolution, achieved by means of the particle splitting technique (Kitsionas & Whitworth 2002). We increase the resolution long before the old resolution limit is reached, so that no spurious numerical effect can influence our results. In the most accurate simulation we can resolve the sphere of influence of each MBH in a self–consistent manner to gain insight on the MBH activity and potential mass growth on sub–parsec scales. For the first time, we present the mass profile of the gas bound to the MBHs, so that we can conjecture on the accretion phase during the MBH pairing and inspiral.

The paper is organized as follows: in Section 2 we describe the initial conditions for the different runs; in Section 3 we present the results of the simulations for different disc/stellar fraction and numerical resolution; in Section 4 we derive our conclusions.

2 SIMULATION SETUP

Simulations are run using the N–Body/SPH code GADGET (Springel, Yoshida, & White 2001). In all our simulations, a MBH with a mass of $4 \times 10^6 M_\odot$ is hosted in the centre of a gaseous+stellar disc, embedded in a larger scale stellar spheroid. The disc is modeled with 235331 particles, has a total mass $M_{\text{Disc}} = 10^8 M_\odot$, and follows a Mestel surface density profile,

$$\Sigma(R) = \frac{\Sigma_0 R_0}{R}, \quad (1)$$

where R is the radial distance, projected into the disc plane, and Σ_0 and R_0 are reference values. The disc is rotationally supported in R , and has a finite radial extension of 100 pc and a finite vertical thickness of 10 pc. The particles are distributed with a initially uniform vertical distribution.

The spheroidal component (bulge) is modeled with 10^5 collisionless particles, initially distributed as a Plummer sphere, i.e., with a mass density profile as

$$\rho(r) = \frac{3}{4\pi} \frac{M_{\text{Bulge}}}{b^3} \left(1 + \frac{r^2}{b^2} \right)^{-5/2}, \quad (2)$$

where b (= 50 pc) is the core radius, r the radial coordinate, and M_{Bulge} (= $6.98 M_{\text{Disc}}$) the total mass of the spheroid. With such choice, the mass of the bulge within 100 pc is 5 times the mass of the disc, as suggested by Downes & Solomon (1998). The number of particles used to model the two components allows a spatial resolution $\simeq 1$ pc, corresponding to the employed gravitational softening which is the same for stellar, gaseous and MBH particles.

We run four different sets of simulations, assuming a purely gas disc, and a disc in which 1/3, 2/3, and, finally, all gas particles are turned into collisionless particles. For any disc considered, we evolve initial condition in isolation until equilibrium is reached. The gaseous component has a initial internal energy density profile

$$u(R) = KR^{-2/3}, \quad (3)$$

where K is a constant defined so that the Toomre parameter of the disc,

$$Q = \frac{\kappa c_s}{\pi G \Sigma}, \quad (4)$$

is > 3 everywhere, preventing fragmentation, and the formation of stable large scale over–densities, such as bars and spiral arms. In equation (4) κ is the local epicyclic frequency, and c_s the local sound speed of the gas, that, for our choice of K , is $\approx 30 \text{ km s}^{-1}$ at $R = 50$ pc. The internal energy of gas particles mimics the internal, unresolved turbulence, and, as a consequence, c_s has to be considered as the local turbulent velocity.

The stellar component in the disc is obtained converting gas particles in collisionless particles. The latter own the same mass and position of the initial gas particles, but their velocities are modified by adding an isotropic component

Table 1. Run parameters

run	$M_{\text{MBH}_1}^*$	$M_{\text{MBH}_2}^*$	M_{Disc}^*	Disc stellar fraction	M_{Bulge}^*	e
A1**	4	4				
A2	4	1	100	0	698	0.7
A3		0.4				
B1		4				
B2	4	1	100	1/3	698	0.7
B3		0.4				
C1		4				
C2	4	1	100	2/3	698	0.7
C3		0.4				
D1		4				
D2	4	1	100	1	698	0.7
D3		0.4				

* Masses are in units of $10^6 M_{\odot}$.

** Last phases of this simulation are run with particle splitting method (see Sect. 3.2).

equal (in modulus) to the local sound speed. Gas particles to be turned into stars are randomly selected, so that the stellar disc component follows the same density distribution of the gas. Gas particles are transformed during a simulation at a constant rate of $\approx 160 M_{\odot} \text{yr}^{-1}$. This rate prevents strong relaxation that could, in principle, change the structure of the disc.

We add, in any initial condition, a second MBH at a separation from the central MBH of 50 pc, on an eccentric orbit with eccentricity $e \simeq 0.7$. We allow the mass of secondary to be 4×10^5 , 10^6 , and $4 \times 10^6 M_{\odot}$, so we have a total of 12 simulations. Main initial parameters are resumed in Table 1. Finally, we performed a simulation at higher resolution, starting from an intermediate output of the equal mass MBH – pure gaseous disc run (run A1). A more detailed description of the initial condition of this last simulation is reported in Section 3.2.

3 RESULTS

3.1 Circularization

Figure 1 shows the MBH relative separation a and eccentricity as a function of time (upper and lower panel respectively) for equal mass binaries (runs “1”) of all four sets. Independently of the fraction of gas–disc particles turned into stars, the secondary MBH spirals down to a distance from the primary of ≈ 4 pc, forming a binary that hardens down to the numerical resolution limit in 5 Myrs. Meanwhile, the eccentricity of the MBH orbit decreases, reaching, at the end of the simulations, values as small as $e \lesssim 0.2$. Such value is not a physical lower limit to e , but, as we will show in Section 3.1, it is merely a numerical artifact related to the finite resolution. Circularization was discussed for a pure gaseous disc in DCH06. Here, we prove that the very same process works

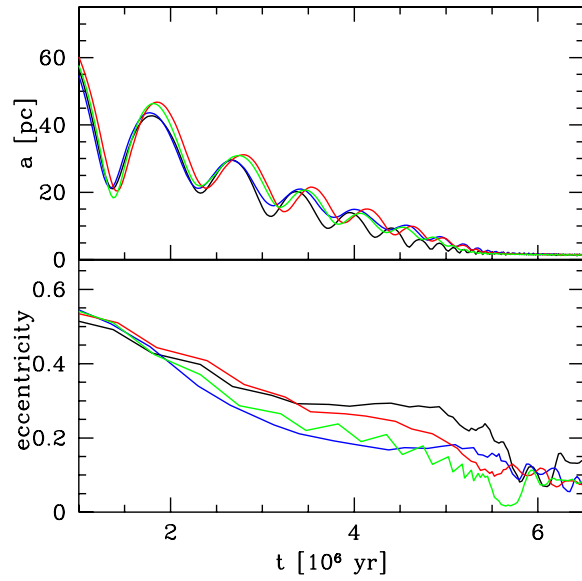


Figure 1. Equal mass MBHs. Upper panel: separations a (pc) between the MBHs as a function of time. Lower panel: eccentricity of the MBH binary as a function of time. Black, blue, red and green lines refer to stellar to total disk mass ratio of 0, 1/3, 2/3 and 1 (run A1, B1, C1, and D1) respectively.

regardless the disc composition, provided that the disc is rotationally supported. This condition is satisfied in DCH06, and in all the runs presented here, as the rotational velocity of the disc is always larger than the gas sound speed and the stellar velocity dispersion.

To show how the circularization process works, consider as an example run C1, where both stellar and gaseous particles form the disc. In Figure 2 we plot the density maps of gas (left panels) and stars (right panels) in the disc at two different times, corresponding to the first passage at pericentre (upper panels), and at apocentre (lower panels). The green curve shows the counterclockwise corotating orbit of the secondary MBH. Near to the pericentre, the MBH has a velocity larger than the local rotational velocity, so that dynamical friction causes a reduction of the (mainly radial) velocity of the MBH. A wake of particles forms behind the MBH trail. On the other hand, around the apocentre, the MBH velocity (mainly tangential) is lower than the disc rotational velocity, and, in this case, dynamical friction increases the MBH angular momentum: the wake is now excited and dragged in front of the MBH trail. Thus, as a result of rotation, the wake reverses its direction at apocentre relative to pericentre, causing circularization (see also Figure 1). This eccentricity evolution is opposite to that occurring in purely collisionless (Colpi, Mayer & Governato 1999; van den Bosch et al. 1999) or in gaseous (Sanchez-Salcedo & Brandenburg 2001) non-rotating spherical backgrounds.

The same circularization process works effectively in the unequal mass cases. Figure 3 shows the MBH separation and eccentricity evolution for a MBH mass ratio of 1/4 (runs “2” for all sets). The color coding is the same as in Figure 1. The drag by friction is in this case weaker and the sinking oc-

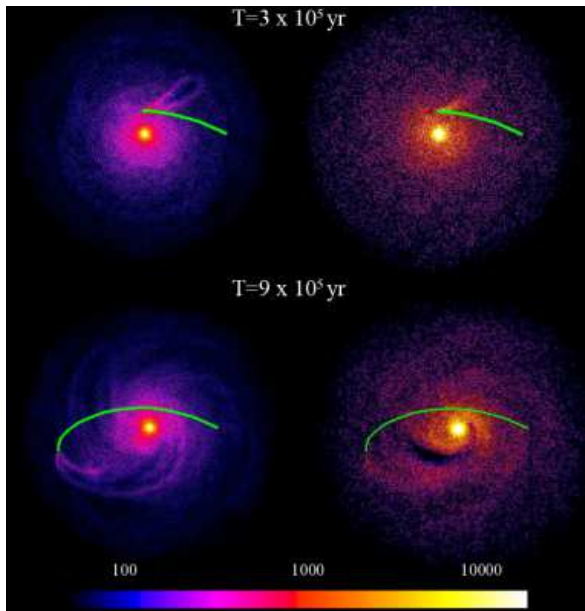


Figure 2. Snapshot from run C1. The panels show a face-on projection of the disk and MBH positions for two different times. The color coding indicates the z -averaged gas density (left panel) and star density (right panel) in logarithmic scale (units: M_\odot/pc^3). The green lines trace the MBH counterclockwise prograde orbits.

curs on a time ≈ 4 longer, scaling with the mass. We can also observe that in the case of a pure gaseous disc (run A2) the circularization process is more efficient compared to all other runs including the stars in the disc. When the secondary MBH moves along the eccentric orbit, its motion is supersonic with respect to the gas and the stars for nearly all the entire orbit. But, for a supersonic perturber, the dynamical friction in a gaseous background is ≈ 2 times more efficient than in a stellar environment (Ostriker 1999). This is accelerating the circularization process. The sinking time instead does not decrease at the same pace as circularization time does, since the deceleration away from the apocentre (higher in a gaseous background) is balanced by the enhance acceleration near apocentre (where the density wake is in front of the MBH trail).

Results of the simulations with MBH mass ratio of 0.1 (runs “3”) are similar to runs “1” and “2”, with relevant times scaling with the inverse of the mass of the secondary. The differences, in runs A3, B3, C3 and D3, in the orbital decay timescale are larger than what we find in runs “1” and “2”, because of the smaller secondary-to-background particles mass ratio. Here a random component of the motion of the secondary MBH exists, mainly caused by the stellar bulge. The mass ratio between the secondary MBH and a bulge particle in runs “3” is 57, so that the background can not be treated as a smooth fluid.

3.2 Nuclear discs around the spiraling MBHs: the high resolution run

We run a higher resolution simulation to study the eccentricity and orbital evolution on scales smaller than 1 pc. The

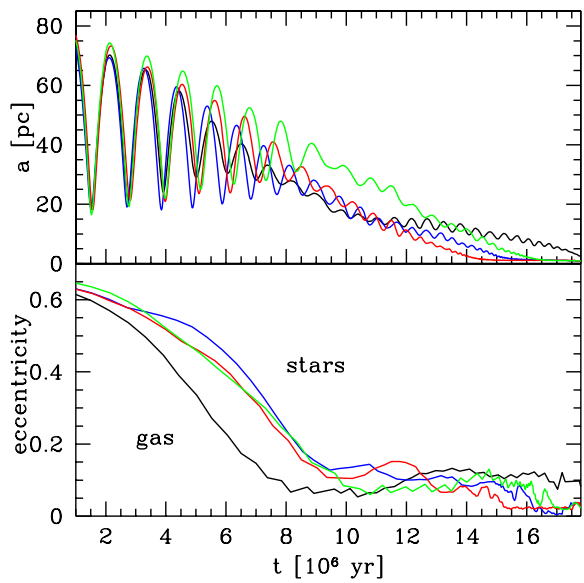


Figure 3. Same as Fig. 1 for MBH mass ratio 1/4 (runs “2” in all sets). Upper panel: separations a (pc) between the MBHs as a function of time. Lower panel: eccentricity of the MBH binary as a function of time. Black, blue, red and green lines refer to stellar to total disk mass ratio of 0, 1/3, 2/3 and 1 (run A2, B2, C2, and D2) respectively.

new initial condition is obtained resampling the output of run A1 with the technique of particle splitting. Resampling is performed when the MBH separation is $a \simeq 14$ pc (corresponding to $\simeq 4$ Myr after the start of the simulation). We split each gas particle into $N_{\text{ch}} = 10$ “child” particles (Kitsonas & Whitworth 2002), randomly distributed around the position of the original parent particle within a volume of size $\sim h_p^3$, where h_p is the gravitational softening (of the parent particle). The velocities of the child particles are taken as equal to that of the parent particle, and so is their temperature. Each child particle has a mass equal to $1/N_{\text{ch}}$ of the mass of the parent. Particle splitting is applied to all particles whose distance from the binary centre of mass is ≤ 42 pc. In this way, the total number of particles increases only by a factor $\simeq 4$, while the local mass resolution in the split region is comparable to that of a standard $\simeq 2 \times 10^6$ particle simulation with uniform resolution. Our choice of the maximum distance for splitting is conservative, and prevents more massive, unsplit gas particles to reach the binary on a timescale shorter than the entire simulation time. The high mass resolution achieved allows a spatial resolution of $\simeq 0.1$ pc in the central region, without any relevant spurious numerical effect. In Figure 4 we compare the surface density profiles of the circum-nuclear gaseous discs in run A1 at $t = 4$ Myrs, for the low and high resolution cases. The two profiles differ only for $R \lesssim 3$ pc from the primary MBH, near the resolution limit of the low resolution simulation. The increase of the spatial resolution corresponds to an enhancement of the MBH gravitational fields, triggering a gas inflow that produces the central cusp observable in the high resolution case. The lack of noticeable differences

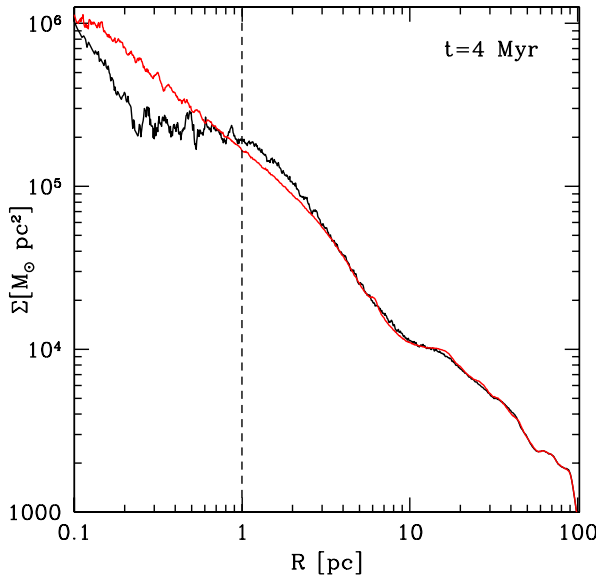


Figure 4. Surface density profile of the circum-nuclear gaseous disc in run A1 at $t = 4$ Myrs. Black line refers to the surface density in the low resolution simulation, red line refers to the high resolution (split) simulation. The dashed vertical line marks the resolution limit in the un-split simulation.

in the surface profile at separation $R > 3$ pc confirms the accuracy of the particle splitting technique.

Results of the high resolution run are shown in Figure 5. The orbital decay does not stall, but rather the separation reaches, in ~ 10 Myrs, a value as low as 0.1 pc, i.e., the new resolution limit. We notice here that the “ellipsoidal torque” regime, defined in Escala et al. 2004 (see also Escala et al. 2005) and characterized by a very fast orbital decay, is not observed. We attribute this difference to the different thermal state of the gas surrounding the MBHs. For a comparison, we rescale the results of our simulation to the ones presented in Escala et al. (2005) to match the values of the masses and extensions of the bulge and disc in the various runs. After the rescaling, our initial disc is hotter by a factor ≈ 2.36 than the hottest disc model presented in Escala et al. (2005). Figure 13 of Escala shows the decrease in the efficiency of angular momentum extraction by the ellipsoidal torque with increasing temperature. If this efficiency decreases linearly with increasing temperature, we can extrapolate a timescale of 3 Myrs for the MBH binary inspiral down to the new resolution limit, comparable to the timescale observed in our simulation. Given the inferred lower efficiency of angular momentum extraction by ellipsoidal torques for “hot” discs (Toomre parameter > 3) the transition between the dynamical friction driven and ellipsoidal torque driven orbital decay is not discernible. The circularization efficiency is increased, with respect to the runs at lower resolutions. The dynamical evolution of the MBHs is affected by the increased resolution long before the binary separation is of the order of the old, unsplit spatial resolution. Because of particle splitting, the system decreases its granularity, and the binary decreases its eccentricity to a

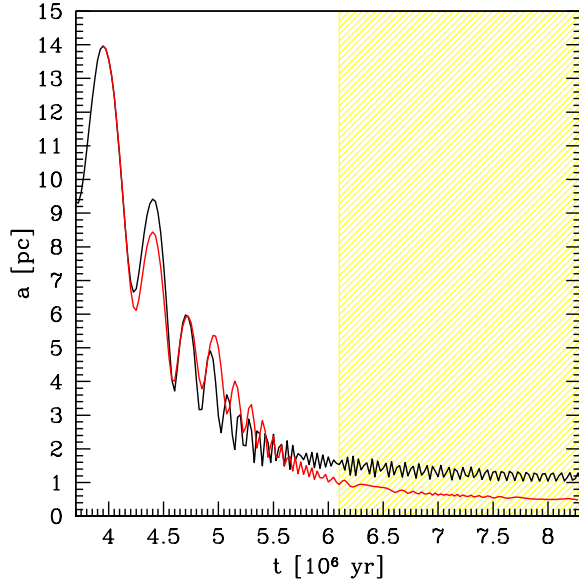


Figure 5. Separations a (pc) between the MBHs as a function of time. Red (black) line refers to the (un-)split run A1. The dashed area highlight when the MBHs separation is < 1 pc (that corresponds to the old numerical resolution) in the split run A1.

value consistent with zero well before the new spatial resolution limit is reached. The small variation in the dynamical friction efficiency at separations $a \lesssim 3$ pc (greater than the old spatial resolution) is likely caused by the increase in the circularization efficiency, and by the increased spatial resolution of the the density profile on the same scales (see Figure 4).

A resolution of 0.1 pc allows to study the properties of the gas bound to each MBH. To this purpose, it is useful to divide bound gaseous particles into three classes, according to their total energy relative to the MBH. We then define weakly bound (WB), bound (B), and strongly bound (SB) particles according to the following rule:

$$E < \begin{cases} 0 & (\text{WB}) \\ 0.25 W & (\text{B}) \\ 0.5 W & (\text{SB}), \end{cases} \quad (5)$$

where E is the particle energy per unit mass, i.e., sum of the kinetic, internal and gravitational energies (per unit mass), the last referred to the gravitational potential W of each MBH. Hereafter WBPs, BPs, and SBPs denote particles satisfying the WB, B, and SB limit, respectively. Note that, with the above definition, SBPs are a subset of BPs, which in turn are a subset of WBPs.

After a short phase following the transit of the system from the old to the new force resolution, equilibrium is restored. From this moment on, each MBH collects a mass of WBPs, BPs, and SBPs of $M_{\text{WB}} \approx 0.85 M_{\text{MBH}} \approx 3.4 \times 10^6 M_{\odot}$, $M_{\text{B}} \approx 0.41 M_{\text{MBH}} \approx 1.6 \times 10^6 M_{\odot}$, and $M_{\text{SB}} \approx 0.02 M_{\text{MBH}} \approx 8 \times 10^4 M_{\odot}$, respectively. In Figure 6 the masses associated to the three different classes of bound gas particles are shown for each individual MBH as a func-

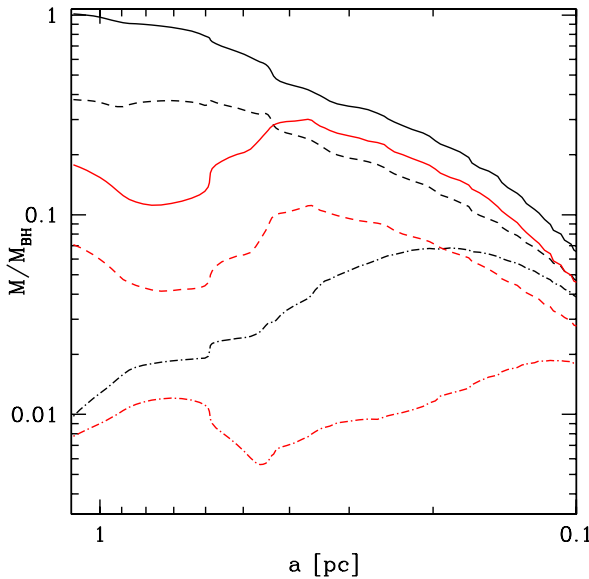


Figure 6. Masses of bound gas particles as a function of binary separation a in the final stages of the higher resolution simulation (slit run A1). MBH separations of 1 and 0.1 pc corresponds to $t \approx 6$ and ≈ 8.5 Myr, respectively (see dashed area in Figure 5). Black lines refer to gas particles bound to the MBH initially at rest, red lines refer to the ones bound to the initial orbiting MBH. Solid, dashed, and dot-dashed lines refer to WB, B, and SB particles.

tion of the binary separation, decreasing from 1 to 0.1 pc over the last ≈ 2 Myrs of the explored evolution.

As the binary shrinks, WBP and BPs are easily perturbed, as illustrated in Figure 6. At the end of the simulation M_{WBP} and M_{BP} are reduced by an order of magnitude. During the same period of time, M_{SB} associated to the primary (secondary) MBH increases instead of a factor ≈ 4 (≈ 2.5). This result is unaffected by the numerical noise since the number of bound particles (associated to each class) exceeds the number of SPH neighbors ($N_{\text{neigh}} = 50$) defined in the simulations. As an example, the SBPs are $> 4 \times N_{\text{neigh}}$ during the entire simulation, so that the mass associated to this component is not biased by a lack in the hydrodynamical resolution.

We expect that as orbital decay continues even beyond our resolution limit, some of the SBPs would also eventually unbind. The radial density profiles of WBPs, BPs, and SBPs are well resolved during the simulation. As an example, in the upper panel of Figure 7 we show, for each individual MBH, the normalized mass within a given distance r_{MBH} from the MBH, for WBPs, BPs, and SBPs, at $t = 4.5$ Myrs, when the binary separation is ≈ 5 pc. M_{class} is M_{WB} , M_{B} , and M_{SB} respectively.

The lower panel of Figure 7 shows the angular momentum component perpendicular to the disc plane of these particles, computed in each MBH frame. Bound particles have a net angular momentum with respect to each individual MBH, and form an ellipsoidal configuration. Each ellipsoidal structures are pressure supported, with an half-mass radius of $\simeq 3$, $\simeq 1$, and $\lesssim 0.2$ pc for WBPs, BPs, and SBPs. The

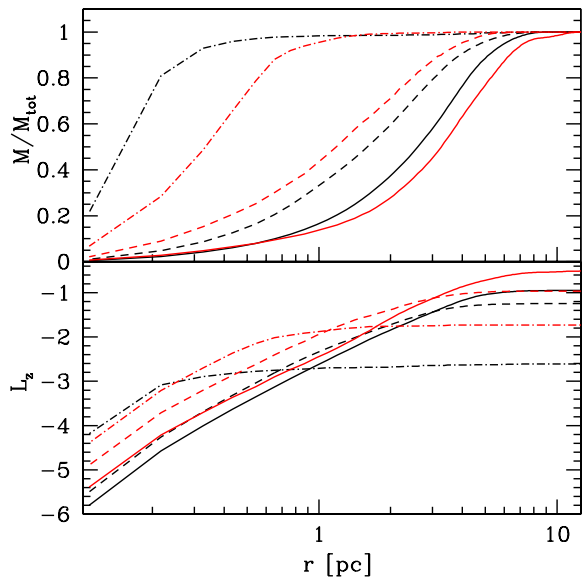


Figure 7. High-resolution simulation at $t = 4.5 \times 10^6$ yrs. Upper panel: z -component of cumulative orbital angular momentum, per unit bound mass, as a function of the distance from each MBH (r). Lower panel: gaseous cumulative mass fraction of bound particles as a function of r . The black (red) lines refer to the initial central primary (orbiting secondary) MBH. Solid, dashed, and dot-dashed lines refer to WBPs, BPs, and SBPs strongly, respectively.

disc gas density can be as high as 10^7 atoms cm^{-3} . It is then conceivable that, for such high values, dissipative processes can be important, possibly reducing the gas internal (turbulent and thermal) energy well below the values adopted in our simulations. To assess the importance of dissipative processes, we estimate the effective radius of a rotationally supported gaseous Keplerian disc carrying an angular momentum comparable to what we found in our split simulation (see Figure 7). From $L_z = \sqrt{G M_{\text{MBH}} r_{\text{MBH}}}$, we obtain, for the primary MBH, an effective radius $R_{\text{MBH,disc}} \approx 0.1$ pc (0.03 pc) for WBPs and BPs, respectively. The secondary MBH is surrounded by particles with a comparatively higher angular momentum (see Figure 7, lower panel). The corresponding effective radius are $R_{\text{MBH,disc}} \approx 1(0.13)$ pc for WBPs and BPs, respectively. For both the primary and the secondary, $R_{\text{MBH,disc}} \ll 0.01$ pc for SBPs, a scale more than an order of magnitude below our best resolution limit. These simple considerations indicate that a more realistic treatment of gas thermodynamics is necessary to study the details of gas accretion onto the two MBHs during the formation of the binary, and the subsequent orbital decay. Nonetheless, our simplified treatment allows us to estimate a lower limit to the accretion timescale, assuming Eddington limited accretion:

$$t_{\text{acc}} = \frac{\epsilon}{1 - \epsilon} \tau_{\text{Edd}} \ln \left(1 + \frac{M_{\text{acc}}}{M_{\text{MBH,0}}} \right), \quad (6)$$

where ϵ is the radiative efficiency, τ_{Edd} is the Eddington time, $M_{\text{MBH,0}}$ is the initial mass of a MBH, and M_{acc} is the mass of the accreted gas. Assuming $\epsilon = 0.1$, accretion can

last at least 27 Myrs, 15 Myrs, and $\lesssim 1$ Myrs, if the MBHs accrete all the WBPs, BPs, and SBPs, respectively.

4 DISCUSSION

In this paper we have shown that dynamical friction against the gaseous and/or stellar background is responsible of the inspiral of the MBH pair inside a massive nuclear disc. A MBH binary forms at a separation $a \sim 5$ pc. The gas and stellar distribution around the MBHs is such that dynamical friction keeps acting on the individual MBHs down to a separation of ≈ 1 pc since the coherence of the density wakes excited by the MBHs is maintained down to this scale. Thanks to the particle splitting technique applied to the case of a purely gaseous disc, we have been able to follow the orbital decay down to ≈ 0.1 pc and to show that angular momentum loss by friction, along co-rotating orbits, is able to reduce the eccentricity to a value consistent with zero.

At the separations explored in this paper, other processes neglected here can act to shrink the MBH binary. Three body encounters with individual stars may become important since the hardening radius below which energy and angular momentum exchanges become efficient is ≈ 0.5 pc for the MBH masses considered in this paper (Quinlan 1996). The cumulative effect of this collisional process, studied in nearly spherical backgrounds, can lead to an increase of the eccentricity thus acting against the circularization driven by the large-scale action of the gaseous and/or stellar disc (Quinlan 1996; Aarseth 2003; Matsubayashi et al. 2005; Berczik et al. 2006; Sesana et al. in preparation). The effect of three body encounters on the MBH orbits when stars form a rotationally supported disc is still unclear.

The last main result of this study concerns the structure of gas particles bound to each individual MBH. We have found that during the orbital inspiral, the gravitational attraction of each MBH on surrounding gas particles is such that about 50% of the MBH mass is conveyed inside the MBH sphere of influence and that 2% of the MBH mass is deeply bound to each single MBH. The mass radial profiles of the most bound gas particles suggest that an active Eddington-limited accretion phase may set in, for a time $\lesssim 1$ Myrs around both MBHs. Since we have neglected gas cooling in the simulation, this mass represents only a lower limit. The active phase could last for a longer time $\gtrsim 10$ Myrs, comparable to the inspiral timescale, if all the nominal bound mass is accreted. This highlights the possibility of revealing double AGN activity, on spatial scales $a \lesssim 10$ pc. However, since we expect that star formation is still ongoing in the disc while the MBHs spiral in, double AGN activity could be obscured and thus difficult to disentangle. In the same high resolution simulation, we have measured the cumulative angular momentum (perpendicular to the disc) of the particles bound to each individual MBH. This enable us to infer for the first time the size of the Keplerian nuclear disc that is expected to form: ≈ 0.1 pc and $\ll 0.01$ pc for the bound and the strongly bound gas components, respectively. The small extension of the nuclear disc around each MBH could preserve the gas against tidal perturbation and stripping until the binary reaches separations of the same order.

We plan to carry on higher resolution simulations with

more realistic input physics and radiative cooling in order to follow the later gas-dynamical evolution of the nuclear discs around the MBHs. In particular we aim at tracing the expected transition of the two discs into a circumbinary disc surrounding the two MBHs.

Armitage & Natarajan (2002) have shown that the interaction between the two MBHs and the circumbinary disc can drive the binary to the coalescence in 10 Myrs, for MBH separations $a \lesssim 0.1$ pc. They have also shown that during this process the MBH binary orbital eccentricity increases even if starting from MBHs in quasi-circular orbits (Armitage & Natarajan 2005). The new simulations will test in a self-consistent way their predictions and explore the possibility of exciting flaring activity during the latest phases of MBH binary inspiral. This will constrain the properties of an electromagnetic precursor associated to the binary coalescence (Armitage & Natarajan 2002; Kocsis et al. 2005; Milosavljevic & Phinney 2005; Dotti et al. 2006).

ACKNOWLEDGMENTS

REFERENCES

Armitage P.J., Natarajan P., 2002, ApJ, 567, L9
 Armitage P.J., Natarajan P., 2005, ApJ, 634, 921
 Aarseth S. J., 2003, Ap&SS, 285, 367
 Ballo L., Braito V., della Ceca R., Maraschi L., Tavecchio F., Dadina M., 2004, ApJ, 600, 634
 Barnes J. E., Hernquist L., 1991, ApJ, 370, L65
 Barnes J. E., Hernquist L., 1996, ApJ, 471, 115
 Bender P. et al. 1994, *LISA, Laser Interferometer Space Antenna for gravitational wave measurements*: ESA Assessment Study Report
 Berczik P., Merritt D., Spurzem R., Bischof H.P., 2006, ApJ, 642, 21
 Brown W.R., Geller M.J., Kenyon S.J., Kurtz M.J., 2006, accepted by ApJ (astro-ph/0604111)
 Bryant P.M., Scoville N. Z., 1999, AJ, 117, 263
 Colpi M., Mayer L., Governato F., 1999, ApJ, 525, 720
 Davies R., Genzel R., Tacconi L., Mueller Sanchez F., Sternberg A., submitted to MNRAS (astro-ph/0612041)
 Dotti M., Colpi M., Haardt F., 2006, MNRAS, 367, 103 (DCH2006)
 Dotti M., Salvaterra R., Sesana A., Colpi M., Haardt F., 2006, MNRAS, tmp 997D
 Downes D., Solomon P.M., 1998, ApJ, 507, 615
 Escala A., Larson R.B., Coppi P.S., Maradones D., 2004, ApJ, 607, 765
 Escala A., Larson R.B., Coppi P.S., Maradones D., 2005, ApJ, 630, 152
 Ferrarese L., et al., 2006, ApJS, 164, 334
 Greve T.R., Papadopoulos P.P., Gao Y., Radford S.J.E., 2006, submitted to ApJ (astro-ph/0610378)
 Hughes S. A., 2002, MNRAS, 331, 805
 Kazantzidis S. et al., 2005, ApJ, 623, L67
 Kitsionas S., Whitworth S., 2002, MNRAS, 330 129
 Kocsis B., Frei Z., Haiman Z., Menou K., 2005, ApJ, 637, 27
 Komossa S., Burwitz V., Hasinger G., Predehl P., Kaastra J.S., Ikebe Y., 2003, ApJ, 582, L15
 Komossa S., 2006, Mem. Soc. Astron. Ital., 77, 733
 Kormendy J., Gebhardt K., Fisher D.B., Drory N., Macchetto F.D., Sparks W.B., 2005, AJ, 129, 2636
 Krajnovic D., Jaffe W., 2004, A&A, 428, 887
 Lopes R.D.S., Storchi-Bergmann T., Saraiva M.F.O., Martini P., ApJ in press (astro-ph/0610380)

Mayer L., Kazantzidis S., Madau P., Colpi M., Quinn T., Wadsley J., 2006, to appear in the Proceedings of the Conference "Relativistic Astrophysics and Cosmology - Einstein's Legacy" (astro-ph/0602029)

Matsubayashi T., Makino J., Ebisuzaki T., 2005, preprint astro-ph/0511782

Milosavljevic M., Merritt D., Armin R., van den Bosch F.C., 2002, MNRAS, 331, 51

Milosavljevic M., Phinney E. S., 2005, ApJ, 622, L93

Morelli L., et al., 2004, MNRAS, 354, 753

Ostriker E., 1999, ApJ, 513, 252

Quinlan G. D., 1996, NewA, 1, 35

Risaliti G., et al., 2006, ApJ, 637, L17

Sanchez-Salcedo F.J., Brandenburg A., 2001, MNRAS, 322, 67

Sanders D.B., Mirabel I.F., 1996, ARA&A, 34, 749

Scoville N.Z., Yun M.S., Bryant P.M., 1997, ApJ, 484, 702

Scorza C., van den Bosch F.C., 1998, MNRAS, 300, 469

Sesana A., Haardt F., Madau P., Volonteri M., 2005, ApJ, 623, 23

Springel V., Yoshida N., White S.D.M., 2001, NewA, 6, 79

Tacconi L.J., Genzel R., Tecza M., Gallimore J.F., Downes D., Scoville N.Z., 1999, ApJ, 524, 732

van den Bosch F.C., Lewis G.F., Lake G., Stadel J., 1999, ApJ, 515, 50

van den Bosch F.C., Jaffe W., van der Marel R.P., 1998, MNRAS, 293, 343

Yu Q., Tremaine S., 2003, ApJ, 599, 1129